LABORATORY TESTING AND NUMERICAL MODELLING OF THE DYNAMIC BEHAVIOUR OF TAGUS RIVER SAND

Miranda, Luís, *LNEC, Lisboa, Portugal, lmiranda@lnec.pt*
Caldeira, Laura, *LNEC, Lisboa, Portugal, laurac@lnec.pt*
Bilé Serra, João, *LNEC, Lisboa, Portugal, biles@lnec.pt*
Barbosa, André, *OSU, Corvallis, Oregon, EUA, andre.barbosa@oregonstate.edu*

ABSTRACT

In this paper, an immersed tunnel case-study, corresponding to a third Tagus river crossing, supported on liquefiable alluvial sands, is presented. Laboratory testing, namely monotonic drained triaxial tests and cyclic undrained torsional tests, is described. Moreover, a constitutive model, as well as the numerical work, essential to its calibration and to identify its most relevant parameters, are presented. Model parameters, their respective reference values and tests performed to determine directly most of the parameters, are introduced. A parameter sensitivity analysis, conducted through numerical simulation of triaxial monotonic drained tests, is defined. Furthermore, a parameter sensitivity analysis through numerical simulation of cyclic undrained torsional tests, implemented both for the pre-liquefaction and liquefaction phases, is described. Finally, some parameters are determined by fitting the model to the laboratory results.

1. INTRODUCTION

Design of a third Tagus river crossing is currently being considered downstream of 25 de Abril Bridge in Lisbon, Portugal, between Algés and Trafaria, corresponding to an immersed tunnel with a length of approximately 2.4 km.

This type of tunnels are usually an interesting alternative from the economical and safety points of view as (Ingerslev, 2007): they are shallow tunnels, which minimizes imposed water-pressures, reduces overall length of the tunnel and contributes to having flatter approach gradients than in bored tunnels; they have versatile cross-sections, which makes them appropriate for highways and combined railway and road traffic; they are suitable for most types of ground, including soft alluvial materials and conditions like loose permeable soils at the sea bottom, where tunnel boring machines use is not recommended; their construction is mostly performed ashore, ensuring high quality.

Many immersed tunnels are built on alluvial formations in earthquake zones and one of the main issues in their safety design is precisely their resistance to foundation liquefaction. As a matter of fact, displacements of an immersed tunnel resulting from a seismic event depend largely on the behaviour of the surrounding ground, namely its stiffness (Ingerslev et al., 1997). These displacements may be amplified by liquefaction and can lead to ground failure if significant loss of soil strength occurs. Consequences of liquefaction may include loss of lateral or vertical support, differential movements or rotations, movements due to shake-down settlement effects (where granular material naturally densifies due to loss of structure) and floatation of the tunnel. Likewise, its uncontrolled movement is undesirable and could lead to overstressing and damage of the structure or leakage of the tunnel joints. Thus, potential occurrence of seismically induced liquefaction in the foundation and prescription of efficient ground improvement measures to avoid it are topics of utmost importance within the third Tagus river crossing project.

This paper summarizes the laboratory and numerical work to calibrate a chosen constitutive model, the Manzari-Dafalias (M-D) model, to the Tagus river sand properties, with the goal of enabling its future application in the scope of the immersed tunnel crossing design.

2. CASE-STUDY

The immersed tunnel considered in this case-study has a roughly rectangular reinforced concrete cross-section of around 40 m x 11 m (width x height), considering two bores with three traffic lanes in each direction and an additional central bore for pedestrian evacuation and services.
The river maximum depth is about 30 m. Furthermore, the immersed tunnel is supported on alluvial Tagus river sands overlaying Miocenic layers of increasing stiffness and strength with depth and a basalt bedrock (Figure 1).

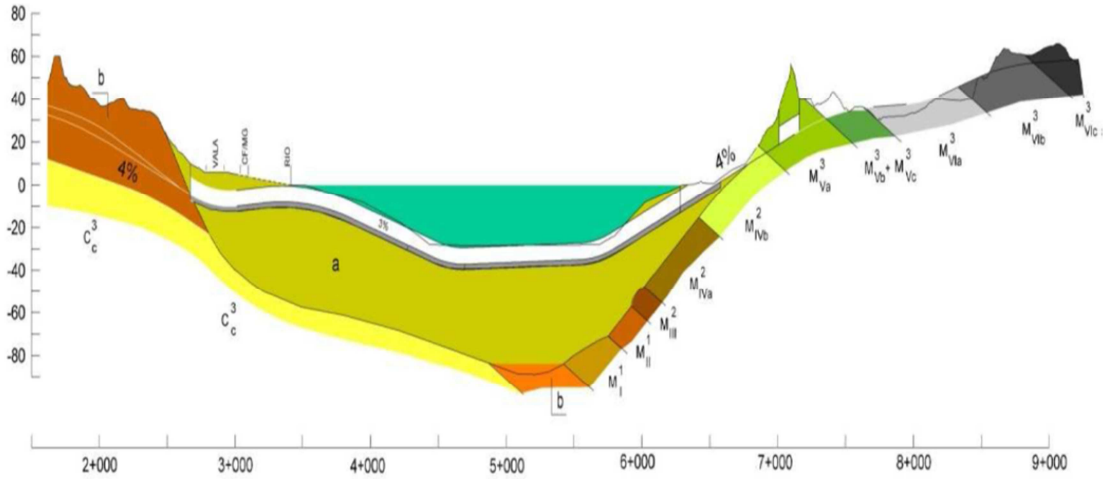

Figure 1 – Third Tagus river crossing geologic profile: a – alluvial Tagus river sands; b – volcanic Lisbon complex; C – Cretacic layers; M –Miocenic layers (Câncio Martins et al., 2001)

Tagus river sand is white, clean and poorly graded (classified as SP). Its physical characterization included: a grain size analysis; determining the solid particles density; and obtaining the maximum, $\gamma_{d,max}$, and minimum, $\gamma_{d,min}$, dry unit weight.
Moreover, the in-situ density index, D_r, of Tagus river sand was determined by using a correlation with SPT values, mainly obtained along the north shore of the river, for different boreholes and depths. Density index was quite constant with depth, at least in the correlation's valid region (up to 20 m). Therefore, a $D_r = 70\%$ after specimen consolidation in the laboratory tests and effective confining pressures p_{conf} going from 100 to 300 kPa were intended, admitting that depth of interest for liquefaction studies is 30 m maximum (σ_v around 300 kPa). What's more, $D_r = 60\%$ ($p_{conf} = 100\,kPa$) and $D_r = 80\%$ ($p_{conf} = 300\,kPa$) were also considered to compare with the other laboratory tests and validate the chosen constitutive model. All stresses herein defined are effective stresses.

3. LABORATORY TESTING

3.1. Monotonic Drained Triaxial Testing

The goal of these tests was characterizing the stress-strain behaviour of Tagus river sand. Moreover, obtaining its basic strength parameters was intended, as well as some plastic modulus and dilatancy-related parameters, paramount to calibrate the used constitutive model.
So, ten monotonic drained triaxial tests (MDTTs) were executed. Table 1 includes dimensions of the specimen, H_0 and r_0 as well as their dry unit weight, γ_d, density index, D_r, and voids ratio after preparation, e_0; and the effective consolidation pressure, p_{conf}, and voids ratio after the consolidation phase, e_{conf}. The accepted density index after preparation was: 70%±2% for tests B, C and D; 60%±2% for test E; and 80%±2% for test J.
Test A was an isotropic consolidation test, with D_r around 70% and p_{conf} of 1000 kPa. Tests F, G and H were also isotropic consolidation tests, in this case with D_r around 60%, used to clarify the cause of some volumetric jumps in the consolidation phase. Finally, test I was made

maintaining p constant, with the goal of determining a dilatancy-related parameter A_0 for the constitutive model (see section 4). These tests won't be presented here.
After the saturation phase, specimens were isotropically consolidated. All tests were then subjected to shear by controlling axial strain, ε_a. During shear, the radial confining pressures were kept constant. The tests were executed with the back pressure drainage valve open, so pore pressure was constant during the test.

Table 1 – Monotonic drained triaxial tests

	After specimen preparation					After consolidation	
Test	$H_0\ (mm)$	$r_0\ (mm)$	$\gamma_d\ (kN/m^3)$	$D_r\ (\%)$	e_0	$p_{conf}\ (kPa)$	e_{conf}
B	119.98	34.73	16.21	71.3	0.634	300	0.584
C	122.96	34.75	16.21	71.3	0.634	200	0.626
D	123.24	34.78	16.21	71.3	0.634	100	0.631
E	122.70	34.79	15.81	57.6	0.675	100	0.671
J	120.50	34.75	16.44	78.8	0.611	300	0.566

Figure 2 sums up the obtained results for **tests B, C, D, E and J**, including curves: $(\delta\varepsilon_a, q/p)$ and $(\delta\varepsilon_a, \delta\varepsilon_v)$. The left graphic confirms quality of the tests as the curves are very similar. In the right graphic, the volumetric strain curve of test C should be between tests B and D curves, and the curve of test J should be under the curve of test B, which didn't happen, from $\delta\varepsilon_a$ approximately 11% or 13%, respectively, due to a possible blockage in the back volume system.

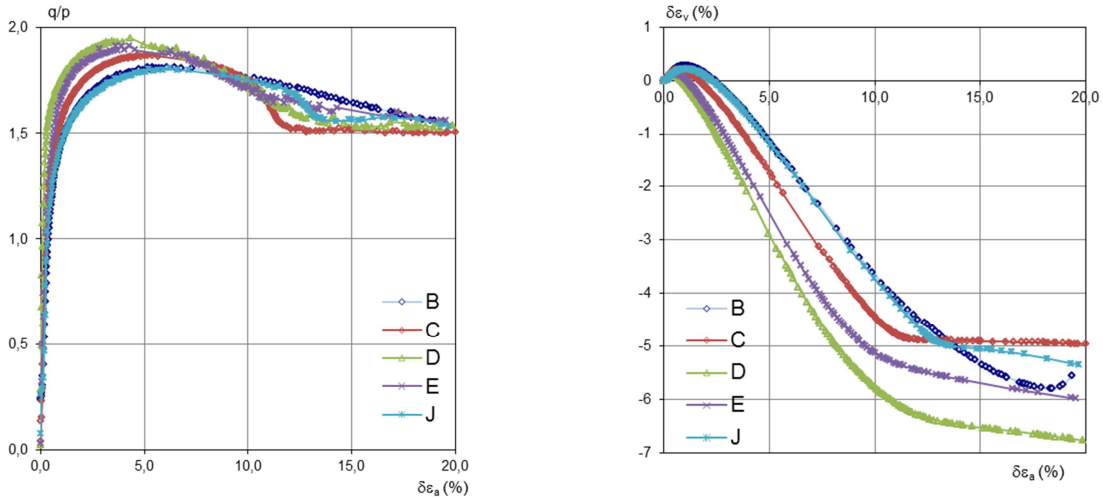

Figure 2 – Tests B, C, D, E and J – stress ratio q/p and volumetric strain $\delta\varepsilon_v$ vs imposed axial strain $\delta\varepsilon_a$

3.2. Cyclic Undrained Torsional Testing

Actuation of the earthquake generates primarily an increase of shear stresses, which can be well simulated in a cyclic torsional test. Thus, the main goal of these tests was to characterize stress-strain behaviour of the sand under cyclic loading and to obtain parameters for the constitutive model, related with dynamic behaviour of the soil.
Therefore, LNEC torsional shear device was used to shear hollow cylindrical specimens. These allowed avoiding solid specimens' non-uniform strain distribution in the radial direction. The equipment is described in more detail in Serra (1998). It's relevant to refer, though, that some changes were made in the software that controls the torsional shear device, namely in the dynamic modulus. In fact, the possibility of changing duration of the test (and number of cycles until test termination), as well as recording data with less than 2 seconds between measured values, was implemented.
In order to assure, as much as possible, homogeneity of stress and strain states along the specimen, so that the corresponding measured average states would correspond to the real

behaviour of the specimen, porous plates at the top and bottom of the specimen were made with a high relief, enhancing friction and better transmitting torsional rotation.

Hence, five cyclic undrained torsional tests (CUTTs) were performed. Table 2 includes dimensions of the specimens, H_0, $r_{e,0}$ and $r_{i,0}$, as well as their dry unit weight, γ_d, density index, D_r, and voids ratio after preparation, e_0; the effective consolidation pressure, p_{conf}, and voids ratio after consolidation phase, e_{conf}. The accepted density index after preparation was: 70%±2% for tests t15, t21 and t22; 60%±2% for test t23; and 80%±2% for test t25.

After the saturation phase, specimens were isotropically consolidated. All tests were subjected to shear by controlling strain $\gamma_{z\theta}$. Rotation amplitude and consequently strain amplitude were increased progressively, using each of the following values during 10 cycles of 1 s ($f = 1Hz$), respectively: $\theta = \pm 0.155°, \pm 0.311°, \pm 0.932°, \pm 1.863°, \pm 3.105°, \pm 6.211°, \pm 9.316°$ and $\gamma_{\theta z} = \pm 5\times10^{-4}, \pm 1\times10^{-3}, \pm 3\times10^{-3}, \pm 6\times10^{-3}, \pm 1.0\times10^{-2}, \pm 2.0\times10^{-2}, \pm 3.0\times10^{-2}$.

Table 2 – Cyclic undrained torsional tests

	After specimen preparation						After consolidation	
Test	$H_0\ (mm)$	$r_{e,0}\ (mm)$	$r_{i,0}\ (mm)$	$\gamma_d\ (kN/m^3)$	D_r (%)	e_0	$p_{conf}\ (kPa)$	e_{conf}
t15	143.14	35.42	14.72	16.15	68.9	0.640	300	0.551
t21	143.34	35.40	14.75	16.17	69.8	0.637	200	0.581
t22	143.09	35.46	14.70	16.18	70.0	0.637	100	0.627
t23	143.14	35.45	14.74	15.92	60.9	0.664	100	0.652
t25	143.30	35.46	14.73	16.51	80.6	0.605	300	0.539

External and internal confining pressures were kept constant (and equal) as well as axial force. Tests were executed with the back pressure drainage valve closed. This implied that changes on the mean effective confining stress were exclusively due to pore pressure development. Moreover, the final excess pore pressure value corresponded approximately to the initial mean effective confining stress, which meant liquefaction was attained in all cases.

For instance, **test t22** has a D_r of 70%, but with the lowest confining pressure of 100 kPa. This means that D_r after consolidation was quite similar to that after specimen preparation. Figure 3 to Figure 5 illustrate the results. Initial liquefaction is considered to have occurred at 46.5 s, similar to t21 and sooner than t15, which may indicate that, for the same D_r, under a certain value, confining pressure doesn't influence significantly time of initial liquefaction.

In Figure 3, for the first cycles the curves are close together, but as the specimen approaches failure strains increase and hysteresis loops' open up quickly. In fact, hysteresis loops' are initially almost vertical, with an area very close to zero and then, after initial liquefaction, they tend to the horizontal, shear strain increasing with very small increase in shear stress.

Concerning Figure 4, the left graph reflects the gradual build-up of pore pressure (Figure 5) as the effective mean stress reduces almost until zero. Thus, when the stress path approaches the critical stress ratio, the specimen starts failing and shape of the stress path changes completely, as seen on the right graph. As a matter of fact, the stress path becomes "hooked" towards the later stages of the test.

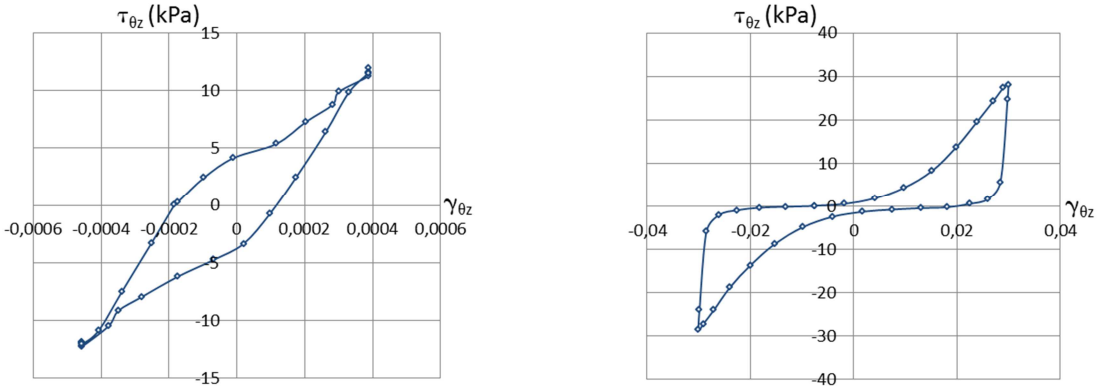

Figure 3 – Shear stress $\tau_{\theta z}$ (kPa) vs shear strain $\gamma_{\theta z}$ – t22 (left - cycle 0-10 s (5 s) (pre-liquefaction); right - cycle 60-70 s (65 s) (liquefaction))

What's more, because of the high pore pressures, the specimen reaches the critical stress ratio at low q values but as strain increases dilation tendency moves the stress path up the critical state line (CSL). When stress reverses, dilation tendency ceases and volumetric contraction tendency drives the stress path back towards the origin until the critical stress ratio is encountered in the opposite (extension) direction.
Finally, in Figure 5 variation of shear strain after initial liquefaction is shown. At 50 s there was a clear transition in the imposed amplitude of shear strain, which was then kept constant and equal to ±2x10^{-2} during 10 s.

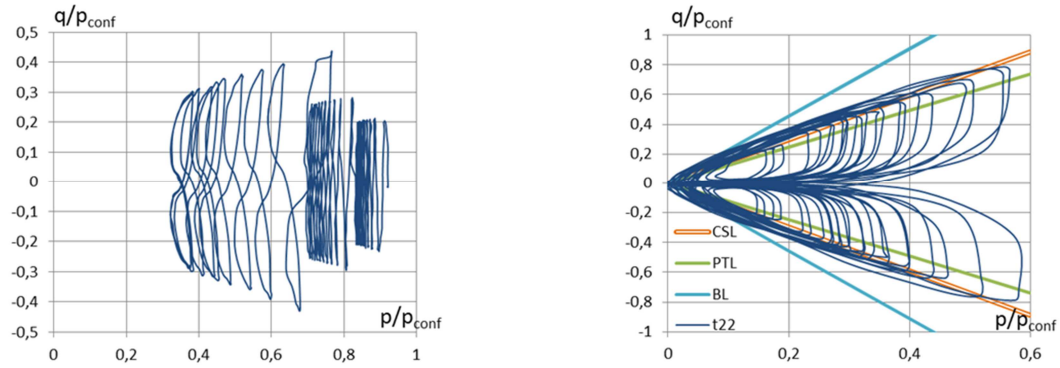

Figure 4 – q/p_{conf} vs p/p_{conf} – t22 (left – 0-30 s (pre-liquefaction); right – after initial liquefaction; CSL – critical state line, PTL – phase transformation line, BL – bounding line)

Moreover, it is fundamental to refer that after a rotation amplitude of 0.932° was imposed (corresponding to a shear strain amplitude of ±3x10^{-3}) sand began to become significantly soft and pp/p_{conf} at the end of the last cycle exceeded approximately 65%.

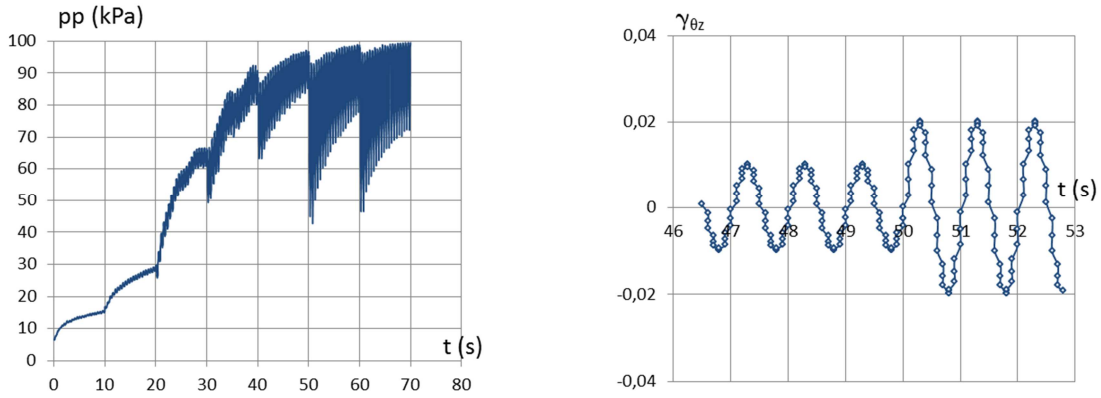

Figure 5 – Pore pressure pp (kPa) and shear strain $\gamma_{\theta z}$ vs time t (s) – t22 (right – after initial liquefaction)

4. NUMERICAL MODELLING OF THE LABORATORY TESTS

4.1. Constitutive Model

The constitutive model has to be capable of reproducing the most relevant aspects of soil behaviour in what concerns cyclic performance and liquefaction. These aspects include liquefaction triggering (contraction tendency with pore pressure build-up), dilatancy effects and post-liquefaction behaviour. The latter shall be well reproduced, as large shear and volumetric deformations in saturated sands take place mostly after initial liquefaction and cause heavy damage in structures. This is essentially due to lateral spreading (mainly near riverbanks) and ground settlement resulting from densification due to dissipation of excess pore water pressures.
The Manzari-Dafalias (M-D) model was chosen. This bounding surface model builds upon previous work by Manzari and Dafalias (1997), which was extended to account for the effect of fabric changes during loading (Dafalias and Manzari, 2004). Therefore, the M-D model is capable of realistically simulating stress-strain behaviour of sands under monotonic and cyclic

loads in drained or undrained conditions. It also allows defining a unique set of model parameters for a given sand, independent of soil density and confining pressure values.
In the formulation in triaxial stress space, the critical state is defined by the critical state stress ratio $q_c/p_c = M_{f,c}$, where parameter $M_{f,c}$ is uniquely related to the friction angle ϕ_f.The following power relation is used for the critical state line (CSL) equation in e-p space:

$$e_c = e_{p0} - \lambda_c (p_c/p_a)^{\xi} \quad [1]$$

with e_{p0} the void ratio at $p_c = 0$, p_a the atmospheric pressure and λ_c and ξ constants. The critical state line in extension is defined by parameters c and $M_{f,c}$.
The **yield surface** represents a ''wedge'' in *p*-*q* space, with an opening value of $2mp$ and whose bisecting line has a slope α (Figure 6). α and m are stress ratio quantities. It is defined as:

$$f = |\eta - \alpha| - m = 0 \quad [2]$$

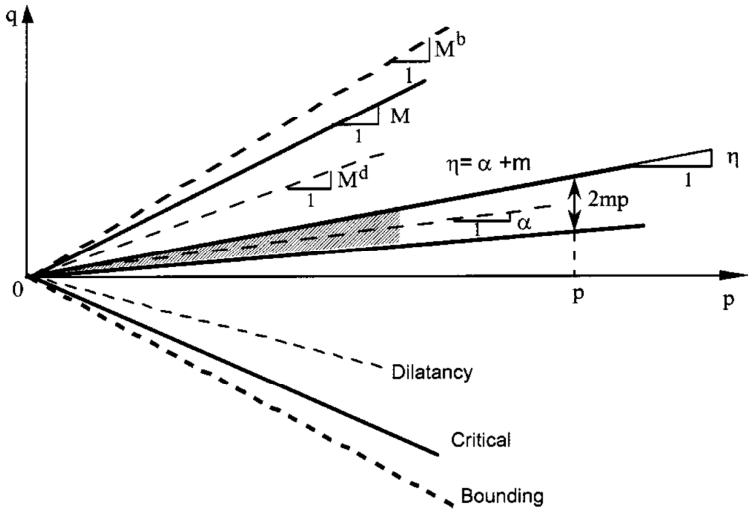

Figure 6 – Yield, critical, dilatancy and bounding lines in *p*-*q* space (Dafalias and Manzari, 2004)

The plastic hardening modulus H_p depends on the state parameter $b = M^b \mp \eta$ where M^b is a peak or bounding stress ratio. For the simplest case of linear dependence:

$$H_p = h\left(M^b \mp \eta\right);\ h = \frac{b_0}{|\eta - \eta_{in}|};\ b_0 = G_0 h_0 (1 - c_h e)\left(\frac{p}{p_a}\right)^{-1/2} \quad [3]$$

with scalar parameters h_0 and c_h. η_{in} is the value of η at initiation of a loading process in compression or the value of h at the point of reversal in extension. Thus, during loading with $d\eta > 0$ one has $H_p = h\left(M^b - \eta\right)$, while for reverse loading with $d\eta < 0$ it changes to $H_p = h\left(M^b + \eta\right)$.
According to Rowe's theory, dilatancy d is proportional to the difference of current stress ratio η from dilatancy stress ratio M^d, also defined as the phase transformation line (PTL):

$$d = A_d\left(M^d - \eta\right) \quad [4]$$

Depending on $\eta < M^d$, $\eta > M^d$ or $\eta = M^d$ a contractant ($d > 0$), dilatant ($d < 0$) or zero volumetric rate ($d = 0$) response is obtained. A corresponding dilatancy stress ratio M^d in extension can be defined, so that $d = A_d\left(M^d + \eta\right)$.

Let a fabric-dilatancy internal variable z and a dependent parameter A_d be introduced:

$$dz = -c_z\langle -d\varepsilon_v^p \rangle (sz_{max} + z) \quad [5]$$

$$A_d = A_0(1 + \langle sz \rangle) \quad [6]$$

where $\langle x \rangle = x$ if $x > 0$ and $\langle x \rangle = 0$ if $x \leq 0$ and $s = \pm 1$ according to $\eta = \alpha \pm m$, respectively. An appropriate variation of M^b and M^d with the material state was also considered, such that when $e = e_c$ and $p = p_c$, then $M^b = M^d = M_{f,c}$. Furthermore, for states denser than critical ($e < e_c$), the condition $M^d < M_{f,c} < M^b$ must hold, and the reverse for states looser than critical. Along these lines, the use of the following equations, with n^b and n^d material constants and $\Psi = e - e_c$, was proposed in Li and Dafalias (2000):

$$M^b = M_{f,c} exp(-n^b \Psi) \quad [7]$$

$$M^d = M_{f,c} exp(n^d \Psi) \quad [8]$$

The model parameters and respective reference values, which correspond either to laboratory tests results ([lab] in Table 3) or to published data in several references about the M-D model [Cheng et al. (2013), Dafalias and Manzari (2004), Papadimitriou et al. (2001), University of Berkeley], plus tests commonly used to determine the parameters, are summarized in Table 3.
The following parameters of the M-D model were directly determined from triaxial monotonic drained tests: $M_{f,c} = 1.46$, $c = 0.67$, $e_{p0} = 0.014$, $\lambda_c = 0.78$ and $\xi = 1.15$ (related with the critical state); $n^b = 3.5$ (related with the plastic modulus) and $A_0 = 0.932$ and $n^d = 1.5$ (related with dilatancy).

4.2. Sensitivity Analysis

The remaining parameters, related to monotonic and cyclic behaviour, were calibrated through numerical simulation of laboratory tests (MDTT and CUTT, respectively). A constitutive driver, developed in OpenSees, was used to perform the simulations. A parameter sensitivity analysis was carried out in order to better understand the relevance of each model parameter.
The selected parameters were those that couldn't be obtained directly by laboratory tests (G_0, m, h_0 and c_h) as well as some parameters that, though obtained directly through laboratory tests, don't have a straight physical meaning (n^b, A_0 and n^d). The intrinsic (physical and critical state parameters) weren't considered for the sensitivity analysis. So, a variation of ±20% of the reference value was defined (except for parameter m, for which it was chosen, according to several references: 0.015, 0.03 and 0.06). This ±20% variation was believed adequate to avoid instabilities and non-convergence of the model. Only the main results of the sensitivity analysis are presented next, since it is described in more detail in Miranda et al. (2017).

4.2.1. Parameter Sensitivity Analysis through Numerical Simulation of MDTTs

An OpenSees model (University of Berkeley) was built to perform the described sensitivity analysis, using a 1x1x1 m^3 SSPbrickUP 3D element with 8 nodes. This element can be used in dynamic analysis of saturated porous media with a mixed displacement-pressure ($u - p$) formulation, based upon the work of Biot as extended by Zienkiewicz and Shiomi (1984).
Regarding boundary conditions, at the base of the element 2 of the 4 nodes were free in each horizontal direction (x and y) and 1 was free in both horizontal directions. The top nodes were all free. During the consolidation phase, concentrated forces representing an all-around confining pressure p_{conf} (100, 200 or 300 kPa) were applied at the free nodes. For the shear

phase of the triaxial test, a vertical displacement (z) was applied at the 4 nodes of the top face of the element, until a vertical axial strain of approximately 20% was reached.

Results of the sensitivity analysis for each model parameter pointed out that the parameters that cause a greater variation of the response are: c_h concerning peak shear strain ε_s, n^b regarding peak shear stress ratio η and finally A_0 concerning peak dilatancy and volumetric strain at the critical state ε_V.

Figure 7 presents the q/p vs $\delta\varepsilon_s$ and $\delta\varepsilon_V$ vs $\delta\varepsilon_s$ graphics considering the effect of varying parameters c_h and A_0, respectively, in the response.

Then, two related parameters (A_0 with n^d concerning dilatancy and c_h with h_0 regarding the plasticity modulus) were varied simultaneously. It was shown that when parameters c_h and h_0 are varied simultaneously, ε_s variation is fairly greater than when only one of them is changed.

Finally, pairs of the most relevant parameters (A_0 with c_h, A_0 with n^b and c_h with n^b), were also varied simultaneously. It was concluded that joint variation of parameters c_h and A_0 causes larger variation than when only one of the parameters is changed.

Table 3 – Manzari-Dafalias model parameters, reference values and published data: [1] - Cheng et al. (2013), [2] - Dafalias and Manzari (2004), [3] - Papadimitriou et al. (2001), [4] - University of Berkeley

Category	Parameter	Reference value	Test
Physical	$\gamma_d(kN/m^3)$	16.21 [lab]	Physical testing
	e_0	0.634 [lab]	Physical testing (Dr = 71.3%)
Elasticity	G_0	125 [4]	RCT (though values from small strain measurements may be 2 or 3 times too large)
	ν	0.3 [lab] ($\phi = 36°$)(0.2 to 0.4 in [3])	$\nu = \frac{K_0}{1+K_0}$ $K_0 = 1 - sin\phi$
Critical state	$M_{f,c}$	1.46 [lab] (1.20 to 1.32 in [3])	MDTT
	c	0.67 [lab]	MDTT ($c = M_{f,e}/M_{f,c}$)
	λ_c	0.014 [lab] (0.01 to 0.03 in [3])	MDTT that approach critical state
	e_{p0}	0.78 [lab] (0.72 to 0.90 in [3])	Void ratio at $p_c = 1kPa$. MDTT that approach critical state
	ξ	1.15 [lab] (0.7 for most sands [1])	MDTT that approach critical state
Yield surface	m	0.015 [4] (0.02-0.05 in [1] and 0.06-0.07 in [3])	Fitting (MDTT)
Plastic modulus	h_0	7.05 [4]	Fitting (MDTT)
	c_h	0.968 [4]	Fitting (MDTT)
	n^b	3.5 [lab] (1.1 in [2])	$n^b = \ln(\frac{M}{M^b})/\Psi^b$, where Ψ^b and M^b are the values of Ψ and η at a drained peak stress ratio state
Dilatancy	A_0	0.932 [lab] (0.704 in [2])	MDTT – good quality stress dilatancy data – volumetric strain vs deviatoric strain in a constant p drained triaxial test (before z is activated $A_0 = A_d$)
	n^d	1.5 [lab] (3.5 in [2])	$n^d = \ln(\frac{M}{M^d})/\Psi^d$, where Ψ^d and M^d are the values of Ψ and η at a phase transformation state
Fabric-dilatancy tensor	z_{max}	4 [4] (4-5 for most sands in [1])	Fitting (CUTT) – η must exceed M^d so that the evolution of z is activated
	c_z	600 [4]	Fitting (CUTT) - η must exceed M^d so that the evolution of z is activated

MDTT - monotonic drained triaxial test; RCT - resonant column test; CUTT - cyclic undrained torsional test.

4.2.2. Parameter Sensitivity Analysis through Numerical Simulation of CUTTs

Here, the consolidation phase was modelled similarly to triaxial tests. Then, in the shear phase, pore pressure was set free at all nodes and top nodes were fixed in the horizontal direction (y). Displacements were applied at the 4 top nodes in the x horizontal direction, according to a cyclic sine function, with a frequency of 1 Hz and which amplitude increases progressively up to ±0.03 m (±1x10^{-5}, ±5x10^{-5}, ±1x10^{-4}, ±5x10^{-4}, ±0.001, ±0.003, ±0.006, ±0.01, ±0.02 and ±0.03 m).

Sensitivity analysis in the pre-liquefaction phase was performed for three different confining pressures: 100, 200 and 300 kPa. Parameters c_z and z_{max} weren't considered in this phase because they only have influence on liquefaction response. From the analysis of 3 cycles gradually approaching liquefaction, it was concluded that the most relevant parameters for cyclic response are G_0, m, h_0 and c_h.

In Figure 8, the normalized stress path q/p_{conf} vs p/p_{conf} for the pre-liquefaction phase and the pore pressure ratio change during the shear phase are shown, considering the effect of changing parameter G_0 in the response.

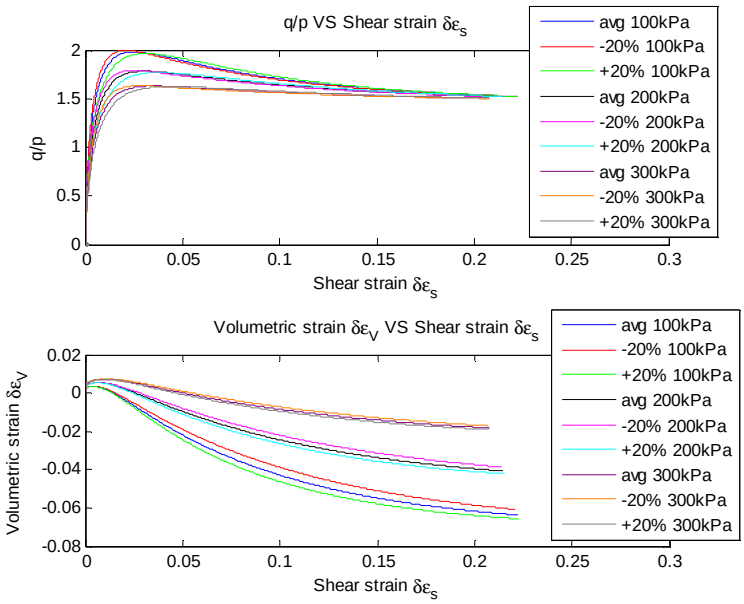

Figure 7 – Simulation results considering variation of a model parameter (up - c_h; down - A_0)

Sensitivity analysis in the liquefaction phase was then performed. In Figure 9, the normalized stress path q/p_{conf} vs p/p_{conf} for 3 cycles in the liquefaction phase is presented, considering the influence of varying c_z in the response. In the liquefaction phase, in each cycle, the pore pressure ratio should reach a value near one and shear strain should follow the applied cyclic displacements. However, due to convergence problems of the M-D model, the pore pressure ratio varies significantly, with its maximum value decreasing and moving away from one and shear strain doesn't follow the applied cyclic displacements (Figure 9). Thus, it wasn't possible to determine the relative importance of c_z and z_{max} in cyclic response. Further improvements in the M-D model are deemed necessary, which are currently underway at the University of Washington, Seattle, through implementation of the PM4Sand model in OpenSees.

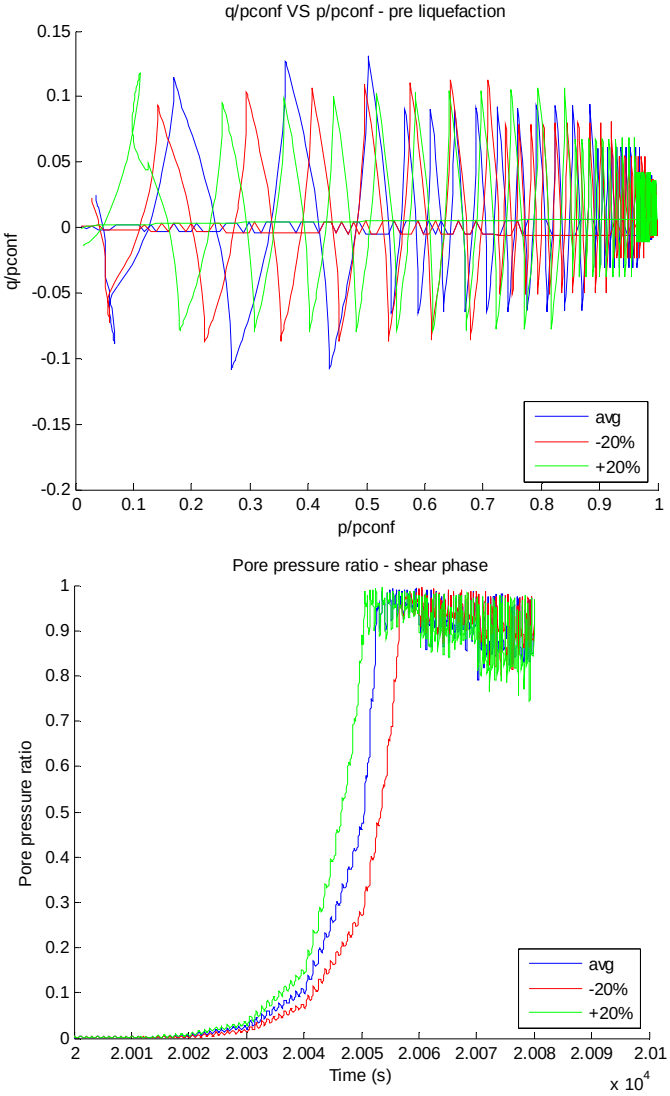

Figure 8 – q/p_{conf} vs p/p_{conf} paths and pore pressure ratio time history considering variation of G_0

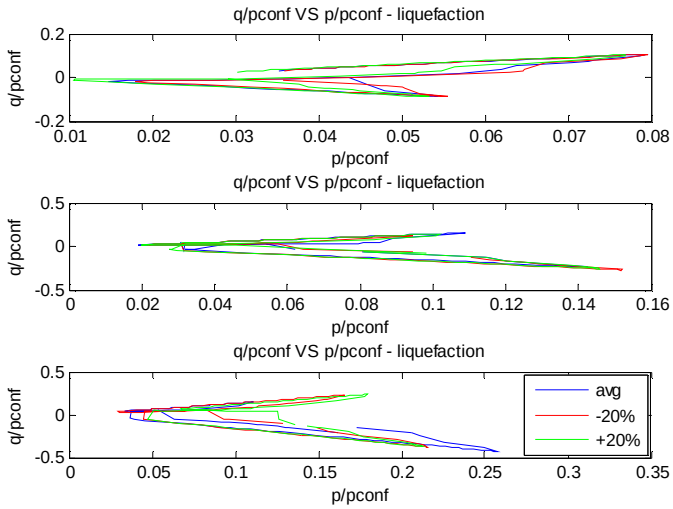

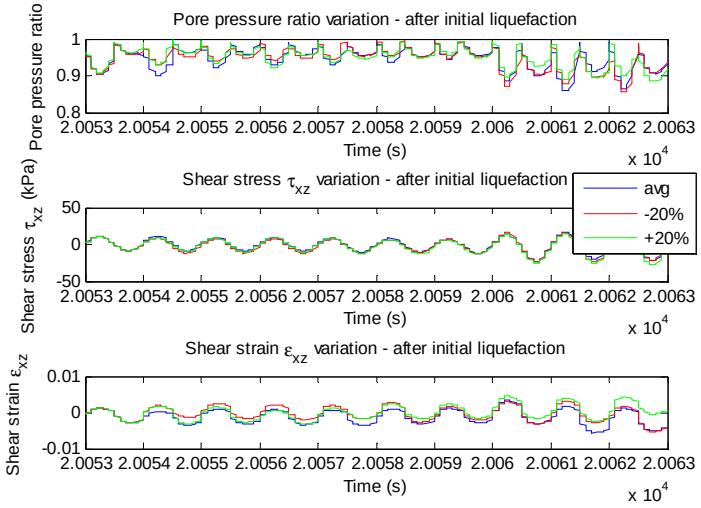

Figure 9 – q/p_{conf} vs p/p_{conf} paths and pore pressure ratio, shear stress and shear strain time history considering variation of c_z

4.3. Fitting the Model to the Laboratory Results

Hence, the value of parameters h_0, c_h and m still had to be determined. This was done by fitting the numerical model to the MDTT results. From the sensitivity analysis, the most relevant of these parameters was c_h and then h_0. Due to its irrelevant influence on the response for the monotonic sensitivity analysis, the used value of m was the reference value in Table 3.
Therefore, parameter c_h was fitted first, followed by h_0. Small adjustments in n^b and A_0 were made as well. As a result, the chosen values for the parameters were: $c_h = 1.33$, $h_0 = 6.05$, $n^b = 4.50$ and $A_0 = 1.25$. These values allowed reproducing the test results for different confining stresses, as shown in Figure 10 for a 200 kPa confining stress.

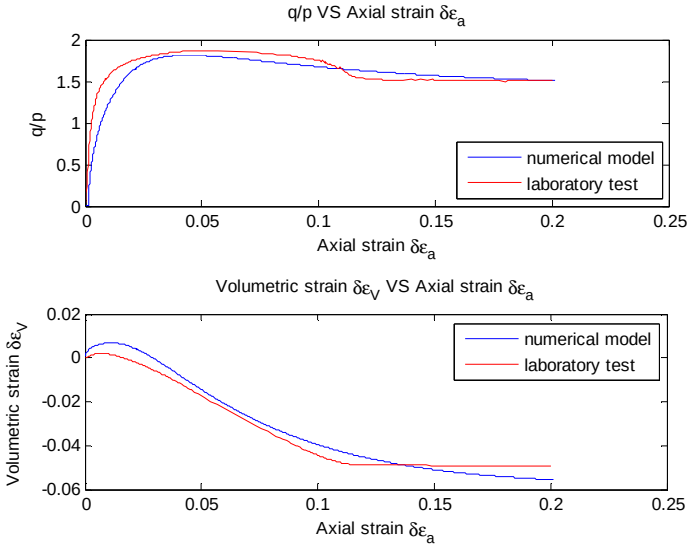

Figure 10 – Fitting MDTT – 200 kPa confining pressure

5. CONCLUDING REMARKS

An immersed tunnel case-study, supported on liquefiable alluvial Tagus river sands, was presented, providing context to this work. Therefore, to characterize stress-strain behaviour of

Tagus river sand and calibrate the M-D model, ten MDTTs were executed. Moreover, five CUTTs were also performed, highlighting dynamic behaviour of the studied sand.
Some parameters of the M-D model were directly determined from triaxial tests, while others (h_0 and c_h) were determined by fitting the model to the laboratory results, after carrying out a sensitivity analysis to understand the relevance of each model parameter. Based on the sensitivity analysis through numerical simulation of MDTTs, it was concluded that the parameters with more importance in the response are c_h, n^b and A_0. In a joint sensitivity analysis c_h and h_0 shall be varied simultaneously, as well as c_h and A_0. Regarding the sensitivity analysis through numerical simulation of CUTTs in the pre-liquefaction phase, it was concluded that the most relevant parameters for the cyclic response are G_0, m, h_0 and c_h.
Both the calibration framework and the results of the sensitivity analysis presented here can provide designers and analysis practitioners with an understanding of the model parameters effects' on its performance and guide them in implementing a complex model into their designs.

ACKNOWLEDGEMENTS

Luís Miranda was supported by "Fundação para a Ciência e Tecnologia" (FCT), through PhD scholarship SFRH/BD/99581/2014. Available geotechnical information from various surveys, namely borehole logs and SPTs, was kindly provided by Administração do Porto de Lisboa.

REFERENCES

Câncio Martins, J. L., Globalvia, Matos Fernandes and Fialho Rodrigues (2001). Travessia Algés-Trafaria em Túnel Imerso.

Cheng, Z., Dafalias, Y. F. and Manzari, M. T. (2013). Application of SANISAND Dafalias-Manzari model in FLAC 3D. *In* Zhu, Detournay, Hart & Nelson (eds.), *Continuum and Distinct Element Numerical Modeling in Geomechanics*, Paper 09-03.

Dafalias, Y. F. and Manzari, M. T. (2004). Simple Plasticity Sand Model Accounting for Fabric Change Effects. *J Eng Mech* 130, pp. 622–634.

Ingerslev, C. (2007). Immersed tunnels state-of-the-art. *Underground Space – the 4th Dimension of Metropolises*, pp. 1493-1498. Barták, Hrdina, Romancov & Zlámal (eds). Taylor & Francis Group, London.

Ingerslev, C. and Kyiomya, O. (1997). Earthquake Analysis. *Tunnelling and Underground Space Technology*, vol. 12(2), pp. 157–162. Elsevier Science.

Li, X. S., Dafalias, Y. F. (2000). Dilatancy for cohesionless soils. *Geotechnique* 50 (4):449–460.

Manzari M. T. and Dafalias Y. F. (1997). A critical state two-surface plasticity model for sands. *Geotechnique*, pp. 255–272.

Miranda, L., Barbosa, A., Serra, J., Caldeira, L. (2017). Parameter sensitivity analysis of the Manzari-Dafalias model for modelling the cyclic response of a sand. *Proceedings of the 16th WCEE*, Santiago, Chile, January 9th to 13th, 2017. https://goo.gl/zhngnq

Papadimitriou, A. G., Bouckovalas, G. D., Dafalias, Y. F. (2001). Plasticity model for sand under small and large cyclic strains. *J Geotech Geoenvironmental Eng* 127, pp. 973–983.

Serra, J. B. (1998). Caracterização experimental e modelação numérica do comportamento cíclico de solos não coesivos. Aplicação à engenharia sísmica. Universidade Técnica de Lisboa. Instituto Superior Técnico. Lisboa, Fevereiro de 1998.

University of Berkeley, California. OpenSees. http://OpenSees.berkeley.edu/ (accessed in several dates).

Zienkiewicz, O. C. and Shiomi, T. (1984). Dynamic behavior of saturated porous media; the generalized Biot formulation and its numerical solution. *International Journal for Numerical Methods in Geomechanics* 8, pp. 71-96.